arXiv:1303.7283v1 [astro-ph.SR] 29 Mar 2013

RESOLVED NEAR-INFRARED SPECTROSCOPY OF WISE J104915.57−531906.1AB: A FLUX-REVERSAL BINARY AT THE L DWARF/T DWARF TRANSITION

Adam J. Burgasser[1], Scott S. Sheppard[2], and K. L. Luhman[3,4]

Submitted to ApJ 27 March 2013

ABSTRACT

We report resolved near-infrared spectroscopy and photometry of the recently identified brown dwarf binary WISE J104915.57−531906.1AB, located 2.02±0.15 pc from the Sun. Low-resolution spectral data from Magellan/FIRE and IRTF/SpeX reveal strong H_2O and CO absorption features in the spectra of both components, with the secondary also exhibiting weak CH_4 absorption at 1.6 μm and 2.2 μm. Spectral indices and comparison to low-resolution spectral standards indicate component types of L7.5 and T0.5, the former consistent with the optical classification of the primary. Relative photometry reveals a flux reversal between the J- and K-bands, with the T dwarf component being brighter in the 0.95–1.3 μm range. As with other L/T transition binaries, this reversal likely reflects significant depletion of condensate opacity across the transition, a behavior that may be enhanced in WISE J1049−5319AB if the unusual red color of its L dwarf component is indicative of thick clouds. On the other hand, differing cloud properties may have modified the evolutionary paths of these two components, and we propose a scenario in which the cooler secondary could be the more massive of the two components. Fortunately, the proximity, brightness and small separation (3.12±0.25 AU) of this system make it amenable to astrometric and radial velocity orbit measurement during its estimated 25 yr orbit, providing a rare opportunity for the direct determination of individual brown dwarf masses and a unique benchmark for studying cloud evolution across the L dwarf/T dwarf transition.

Subject headings: binaries: visual — stars: individual (WISE J104915.57−531906.1) — stars: low mass, brown dwarfs —

1. INTRODUCTION

The low temperatures and luminosities of brown dwarfs near the Sun are a consequence of their age and inability to sustain core hydrogen fusion (Kumar 1962; Hayashi & Nakano 1963). As these objects evolve down the spectral sequence (through the M, L, T and Y spectral classes; Kirkpatrick 2005), their spectral energy distributions become increasingly complex as molecular compounds come to dominate photospheric opacity. These compounds include condensed species: minerals and metals in late-M and L dwarf atmospheres (Lunine et al. 1989; Tsuji et al. 1996), sulfide and alkali salts in late-T and Y dwarf atmospheres (Burgasser et al. 2010b; Morley et al. 2012). Grain scattering and absorption from these condensates cause significant redistribution of flux, veiling of molecular bands, changes in the gas chemistry, modification of cooling rates, and even variability if the condensates are not uniformly distributed in the photosphere (Allard et al. 2001; Ackerman & Marley 2001; Burrows & Sharp 1999; Saumon & Marley 2008; Radigan et al. 2012). Models of cool atmospheres parameterizing "cloudiness" are now used in fits of brown dwarf spectra (Stephens et al. 2009), and condensate clouds are also seen as playing a major role in shaping the spectra of directly imaged giant exoplanets (Currie et al. 2011; Barman et al. 2011; Skemer et al. 2012; Marley et al. 2012).

Discerning the parameters relevant to condensate formation and evolution in cool atmospheres is partly hindered by uncertainties in the characteristics of individual brown dwarfs, which for a given spectral type can span a broad range of age, mass and composition. Resolved brown dwarf binaries have proven to be useful in this regard, as their common distance and genesis eliminates many of the uncertainties in their (relative) physical and spatial characteristics. Such systems are also amenable to direct mass measurement (e.g., Lane et al. 2001; Dupuy et al. 2009; Konopacky et al. 2010), allowing direct comparison to and tests of evolutionary models. Binaries with L dwarf and T dwarf components have been particularly valuable in probing the disappearance of mineral clouds at this spectral transition. A handful are found to be "flux-reversal" pairs, in which the later-type secondary is brighter in the 1.0–1.3 μm region than its earlier-type (and overall more luminous) primary (Burgasser et al. 2006b; Liu et al. 2006; Looper et al. 2008a). These binaries validate the 1 μm brightening found in near-infrared color magnitude diagrams of field L and T dwarfs (the "J-band bump"; Tinney et al. 2003), and suggest that this brightening may be a general feature of brown dwarf evolution. Physical interpretation of this brightening remains under debate, however. It may be evidence of a rapid and/or patchy disruption of the condensate cloud layer (Burgasser et al. 2002; Knapp et al. 2004) or it may reflect variation among sources due to metallicity, mass, age, rotation or other physical characteristics (Burrows et al. 2006). Unfortu-

[1] Center for Astrophysics and Space Science, University of California San Diego, La Jolla, CA 92093, USA; aburgasser@ucsd.edu
[2] Department of Terrestrial Magnetism, Carnegie Institution of Washington, 5241 Broad Branch Rd. NW, Washington, DC 20015, USA
[3] Department of Astronomy and Astrophysics, The Pennsylvania State University, University Park, PA 16802, USA
[4] Center for Exoplanets and Habitable Worlds, The Pennsylvania State University, University Park, PA 16802, USA

nately, binaries straddling the L dwarf/T dwarf transition are relatively rare, and the compact separations typical of brown dwarf pairs (1–10 AU; Burgasser et al. 2007) means that they must be very near to the Sun to be resolved.

The recent discovery of the brown dwarf binary WISE J104915.57−531906.1AB (hereafter WISE J1049−5319AB; Luhman 2013), at a distance of only 2.02±0.15 pc from the Sun, therefore represents an outstanding opportunity to study the L/T transition in considerable detail. Luhman (2013) presented an optical spectrum of WISE J1049−5319A[5] consistent with a spectral type of L8±1 and revealing the presence of strong Li I absorption, implying that this component has a mass below 0.065 $M_{\odot}$ (Rebolo et al. 1992; Magazzu et al. 1993). The observation that the secondary is fainter in the red optical ($\Delta i = 0.45$) indicates that this component could be a late-L or T dwarf. In this article, we report resolved near-infrared photometry and spectroscopy of the WISE J1049−5319AB system using the Folded-Port Infrared Echellette (FIRE; Simcoe et al. 2008, 2010) on the Magellan 6.5m Baade Telescope at Las Campanas Observatory, and the SpeX spectrometer (Rayner et al. 2003) on the 3.0m NASA Infrared Telescope Facility (IRTF). In Section 2 we describe our observations and reduction procedures; in Section 3 we analyze the data, determining component spectral types and magnitudes, and identify the "flux reversal" nature of the system. We discuss our results in Section 4, placing the components of WISE J1049−5319AB in context with other late-L and T dwarfs, examining the role of cloud thickness in the flux-reversal nature and evolutionary history of this system, and motivate mass measurements based on updated predictions of its orbital properties.

2. OBSERVATIONS

2.1. Magellan/FIRE Prism Spectroscopy and Imaging

WISE J1049−5319 was observed with Magellan/FIRE on 12 March 2013 (UT) in photometric conditions with seeing of 0″.8 at J-band. We deployed both the cross-dispersed echelle mode ($\lambda/\Delta\lambda \approx 6000$) and prism-dispersed mode ($\lambda/\Delta\lambda \approx 300$) with the 0″.6 wide slit aligned to the parallactic angle. However, due to a slit motor error, only the prism-dispersed data were useable. Each component was placed separately in the slit, and a series of 1 s exposures (10 for the SE component, 8 for the NW component) were obtained for each in an ABBA dither pattern, nodding 9″ along the 30″ slit. We also observed the A0 V star HD 99338 ($V = 8.26$) in six 1 s nodded exposures. NeAr and quartz lamp exposures, reflected off of the Baade secondary screen, were obtained with the target and A0 V stellar observations for wavelength and pixel response calibration, respectively. Data were reduced using the FIREHOSE low-dispersion reduction package (*firehose_ld*), which produces a 2D estimate of the sky spectrum to remove the background in each exposure (Kelson 2003), determines a 2D wavelength mapping from the NeAr arc exposure, and extracts 1D source and A0 V spectra and variances. Modified routines from

the SpeXtool package (Cushing et al. 2004) were used to scale and combine the individual spectra, correct for telluric absorption and apply a relative flux calibration following the procedures described in Vacca et al. (2003). Signals-to-noise (S/N) for both components peaked at ≈400 in the K-band region.

We also obtained a resolved image of the binary using FIRE's acquisition camera, which has a 50″×50″ field of view (FOV), a pixel scale of 0″.147, and a fixed MKO[6] J-band filter. Several 1 s exposures were obtained with the binary on and off slit; these were median-combined to produce an overall sky frame that was subtracted from all images. We extracted a 9″.7×9″.7 (49×49 pixels) subframe from a single image in which the binary is well-separated from the slit, shown in Figure 1 and analyzed below.

2.2. IRTF/SpeX Spectroscopy and Imaging

WISE J1049−5319 was observed with IRTF/SpeX on 15 March 2013 (UT) in cloudy and windy conditions with poor and variable seeing (1″.5-2″.0 at J-band). We deployed the 0″.5 slit and prism-dispersed mode to obtain $\lambda/\Delta\lambda \approx 120$ spectra covering 0.7–2.5 μm. In this case, the slit was aligned along the binary axis (position angle of 5°, 50° off parallactic) to obtain concurrent spectra, and six 90 s exposures were obtained in an ABBA dither pattern at an airmass of 3.3–3.4. We also observed the A0 V star HD 92518 ($V = 6.87$) at an airmass of 3.3 with the slit aligned to the same position angle. Internal flat field and Ar arc lamp exposures were obtained for pixel response and wavelength calibration. Data were reduced using SpeXtool, applying standard settings. Due to the poor seeing, we did not attempt to extract component spectra; rather, we extracted the combined-light spectrum of the binary using a wide aperture. Average S/N was roughly 400 in the J, H and K-band peaks, respectively. While combining the individual spectral frames, we verified that the variable cloud extinction during the observation was grey and had minimal impact on the observed spectral shape; however, differential color refraction may still be an issue, and is addressed below.

We obtained images of the binary on the same night using the SpeX slit-viewing camera (60″×60″ FOV, pixel scale 0″.12) in each of the MKO J, H and K filters, with the instrument oriented at a position angle of 0°. Four exposures were obtained in each filter using a two-point dither pattern with a 7″ nod, with total integrations of 32 s, 56 s and 84 s, respectively. We interleaved these with observations of a nearby red star 2MASS J10490107−5317252 ($J = 10.75$, $J − K_s = 1.16$) for point spread function (PSF) calibration. Frames were pair-wise subtracted to remove sky background, mirror-flipped along the y-axis to reproduce sky orientation, and 9″.7×9″.7 (81×81 pixels) subframes were excised for analysis. The frames with the best seeing in each of the filters are shown in Figure 1.

3. ANALYSIS

3.1. Spectral Characteristics of WISE J1049−5319

The reduced FIRE spectra of the WISE J1049−5319AB components are shown in

---

[5] We follow the convention of Luhman (2013), labeling the southeastern component A and the northwestern component B based on their relative i-band magnitudes.

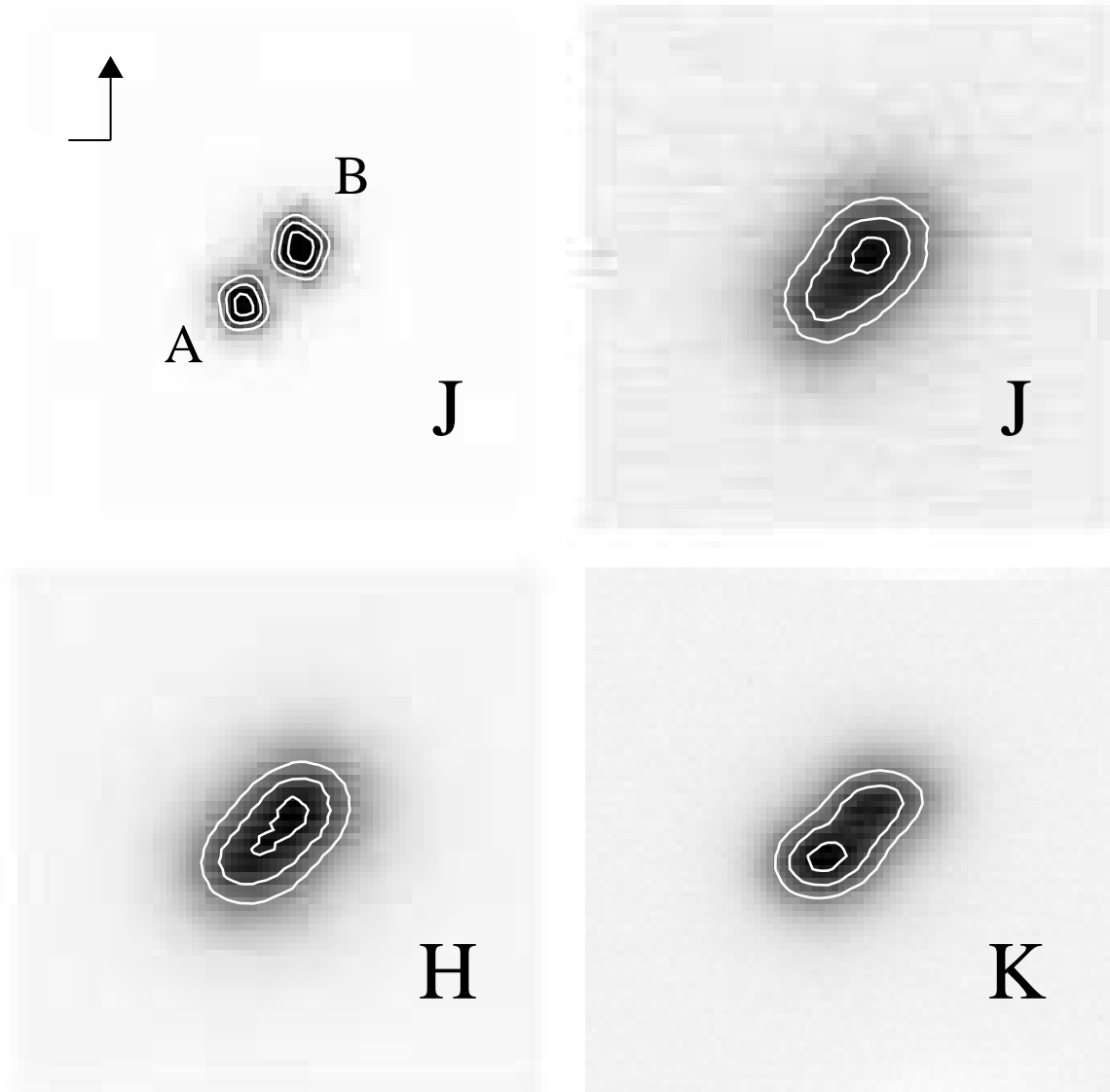[6] Mauna Kea Observatory filter system; see Tokunaga et al. (2002) and Simons & Tokunaga (2002).

FIG. 1.— FIRE (upper left frame) and SpeX slitviewer images of the WISE J1049−5319AB pair in MKO J, H and K-bands (labeled). All three images are oriented with North up and East to the left, and display $9\rlap{.}''7 \times 9\rlap{.}''7$ fields-of-view. Contours are indicated at 50%, 75% and 95% peak flux in the FIRE image, and 50%, 70% and 90% peak flux in the SpeX images. The individual components are labeled in the FIRE image.

Figure 2, scaled to their inferred absolute flux densities as described below. Strong absorption features typical of late-L type brown dwarfs are present, notably deep H_2O bands at 1.4 and 1.9 μm; strong CO absorption at 2.3 μm; marginally resolved Na I and K I doublets at 1.14, 1.17 and 1.25 μm; and a steep 0.8–1.1 μm spectral slope, shaped primarily by the pressure-broadened red wing of the 0.77 μm K I doublet (Burrows et al. 2000). WISE J1049−5319B also exhibits weak absorption from CH_4 at 1.6 μm and 2.2 μm, characteristic of an early-type T dwarf (Burgasser et al. 2006a). Enhanced absorption at 1.15 μm can also be attributed in part to CH_4 absorption. The near-infrared K I lines are stronger in the spectrum of this component, and a hint of FeH can be seen at 0.99 μm (the Wing-Ford band). The overall near-infrared spectral energy distribution of WISE J1049−5319B is bluer than that of WISE J1049−5319A.

Spectral classifications were determined through spectral indices and comparison to spectral standards. We used the indices and spectral type/index relations defined by Geballe et al. (2002); Burgasser et al. (2006a), and Burgasser (2007); values are listed in Table 1. We find mean classifications of L7.5±0.9 and T0.5±0.7, consistent with the characteristics described above; the former is also consistent with the L8±1 optical classification of WISE J1049−5319A reported in Luhman (2013). We then compared the 0.9–1.4 μm spectra to low-resolution spectral standards defined in Kirkpatrick et al. (2010), following the prescription for near-infrared classification outlined in that work. The best-match standards for WISE J1049−5319A and B are the L8 2MASSW J1632291+190441 (Kirkpatrick et al. 1999) and the T1 SDSSp J083717.22−000018.3 (Leggett et al. 2000), respectively (Figure 3); these are consistent with the index types. Note that both components have sig-
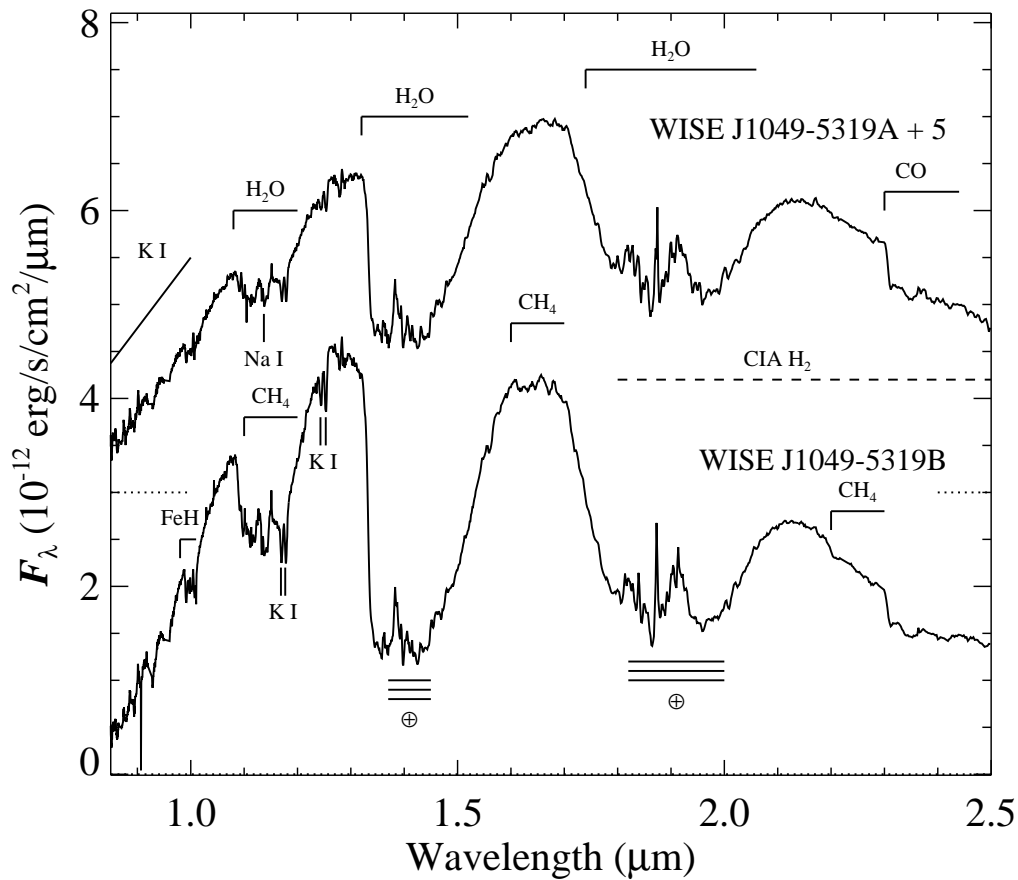
FIG. 2.— Reduced FIRE prism spectra of WISE J1049−5319A (top) and B (bottom), both calibrated to absolute flux units. WISE J1049−5319A is offset by 5×10^{-12} erg s^{-1} cm^{-2} μm^{-1} as indicated by the dotted lines. Major absorption features are labeled, as well as regions of strong telluric absorption ($\oplus$).
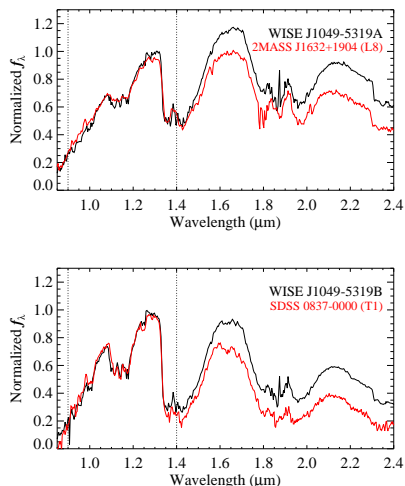

FIG. 3.— Comparison of the FIRE prism spectra of WISE J1049−5319A (top) and B (bottom, in black) to best match near-infrared spectral standards 2MASSW J1632291+190441 (L8) and SDSSp J083717.22-000018.3 (T1, in red), following the method of Kirkpatrick et al. (2010). All spectra are normalized. The comparison region of 0.9–1.4 μm is indicated; both sources are notably redder than their comparison stars. SpeX data for the standards are from Burgasser et al. (2006a) and Burgasser (2007).

nificantly redder spectral energy distributions than their corresponding standards. Finally, we compared the full 0.9–2.4 μm FIRE spectra to low-resolution templates from the SpeX prism Spectral Libraries[7]. We found best matches to the L8 SDSSp J085758.45+570851.4 and the L9.5 SDSSp J083008.12+482847.4 (Geballe et al. 2002) for WISE J1049−5319A and B, respectively, and mean near-infrared classifications of L7±0.9 and L9.5±0.5. Combining these analyses, we assign classifications of L7.5 and T0.5 for the two components, which places them squarely across the L/T transition.

3.2. Component Photometry: A Flux Reversal Binary

Resolved photometry by Luhman (2013) identified WISE J1049−5319A as the brighter of the two sources at i-band, but inspection of the images in Figure 1 indicates that the two components "flip" in relative brightness, with WISE J1049−5319B being brighter at J but fainter at K (WISE J1049−5319B appears to be marginally brighter at H as well). To quantify the amplitude of this reversal, we performed PSF-fitting analyses on our FIRE and SpeX images using a Monte Carlo Markov Chain (MCMC) technique. For the FIRE image, our

---

[7] http://www.browndwarfs.org/spexprism; see Burgasser et al. (2010a) for details.

TABLE 1
CLASSIFICATION INDICES FOR WISE J104915.57−531906.1AB

| | WISE J1049−5319A | | WISE J1049−5319B | | |
Index	Value	SpT	Value	SpT	Ref
H$_2$O-J	0.672±0.010	L8	0.588±0.010	T0.5	1
CH$_4$-J	0.870±0.010	⋯	0.734±0.010	⋯	1
H$_2$O-H	0.681±0.010	L8	0.574±0.010	T0.5	1
CH$_4$-H	1.093±0.010	⋯	1.073±0.010	T1	1
H$_2$O-K	0.716±0.010	L7	0.643±0.010	T1	1
CH$_4$-K	0.936±0.010	⋯	0.845±0.010	⋯	1
H$_2$O-1.2	1.519±0.010	⋯	1.734±0.010	T1	2
H$_2$O-1.5	1.751±0.010	L8	2.213±0.010	T1	2
CH$_4$-1.6	1.073±0.010	⋯	1.093±0.010	T1	2
CH$_4$-2.2	1.068±0.010	L6	1.183±0.010	L9	2
K/J	0.903±0.010	⋯	0.578±0.010	⋯	1
Index Mean	⋯	L7.5±0.9	⋯	T0.5±0.7	⋯
Core Spectral Match	⋯	L8±0.5	⋯	T1±0.5	3
Full Spectral Match	⋯	L7±0.9	⋯	L9.5±0.5	4
Adopted Types	⋯	L7.5	⋯	T0.5	⋯

REFERENCES. — (1) Burgasser et al. (2006a); (2) Geballe et al. (2002); (3) Kirkpatrick et al. (2010); (4) Based on comparison to SpeX templates and using near-infrared spectral types as computed in Burgasser (2007).

PSF model was a 2D ellipsoidal gaussian for which the major and minor axes were allowed to vary separately in width and orientation. For the SpeX images, we used both gaussian profiles and images of the PSF star obtained in the same filter as independent checks, and found that the PSF star provided much more robust fits. Following initial guesses for the pixel positions of both primary and secondary components and their integrated fluxes, our code explored the model parameter space (including gaussian PSF shape) in randomized steps drawn from a normal distribution, and compared model and data at each step using the χ^2 statistic. Sub-pixel shifts for the SpeX PSF model were made using a damped sinc function based on code developed by John Spencer and Mike Ressler. We found that chain lengths of 2000 (with a 200 step burn-in) were sufficient for convergence. For the FIRE analysis, we marginalized the distribution of each parameter in the single chain to determine uncertainties, and included a 5% systematic uncertainty to account for the non-gaussian PSF shape. For the SpeX analysis, we used the mean and standard deviation of the 16 binary and PSF image pairings in each filter as our overall measurement and uncertainty. Separations and position angles from all four image sets were averaged after weighting by individual uncertainties.

Results from these fits are listed in Table 2. The relative photometry confirms the observed flux reversal: WISE J1049−5319B is 0.31±0.05 mag brighter at J (combination of FIRE and SpeX analyses), 0.02±0.06 mag brighter at H (a marginal detection) and 0.29±0.16 mag fainter at K. The reversal at J is highly significant, although not as extreme as that reported for the T1+T5 binary 2MASS J14044941−3159329AB (Looper et al. 2008a; Dupuy & Liu 2012; $\Delta J = -0.54 \pm 0.08$). Figure 4 displays the relative fluxes of the two components optimally scaled according to the relative magnitudes. WISE J1049−5319B is significantly brighter than WISE J1049−5319A between 0.95 μm and 1.3 μm, most notably at the 1.05 μm Y- and 1.27 μm J-band peaks, where the excessive flux reaches 40%.

TABLE 2
RELATIVE PHOTOMETRY FOR
WISE J104915.57−531906.1AB

Parameter	A	B	Δ
ρ ($''$)	⋯	⋯	1$''$54±0$''$04
ρ (AU)	⋯	⋯	3.12±0.25
PA (°)	⋯	⋯	313°±3°
MKO J[a]	11.53±0.04	11.22±0.04	−0.31±0.05
MKO H	10.37±0.04	10.39±0.04	−0.02±0.06
MKO K	9.44±0.07	9.73±0.09	0.29±0.16
M_J	15.00±0.17	14.69±0.17	⋯
$J - K$	2.08±0.08	1.49±0.10	⋯

[a] Uncertainty-weighted average from FIRE (−0.30±0.05) and SpeX (−0.34±0.14) analyses.

WISE J1049−5319B is also marginally brighter across the 1.55–1.7 μm H-band peak. Importantly, these are the wavebands where condensate scattering opacity plays a prominent role in shaping brown dwarf spectra (Ackerman & Marley 2001). As shown in Figure 4, the sum of these scaled spectra are an excellent match to the combined light SpeX spectrum of the binary, which required modest reddening ($A_V = 0.6$) to reproduce the combined light colors, likely to account for differential color refraction at the high airmass of the observation.

4. DISCUSSION

Our relative photometry allows us to infer individual component magnitudes and colors for WISE J1049−5319AB and place them on color-magnitude diagrams, as shown in Figure 5. As in our comparison with the spectral standards (Figure 3), we see that both components are relatively red and subluminous for their spectral types, with WISE J1049−5319A in particular being one of the reddest L dwarfs with a well-determined parallax. Unusually red $J - K$ colors for L dwarfs have been attributed to youth (Kirkpatrick et al. 2006), unusually thick clouds (Looper et al. 2008b) or both (Currie et al. 2011; Faherty et al. 2013). The kinematics
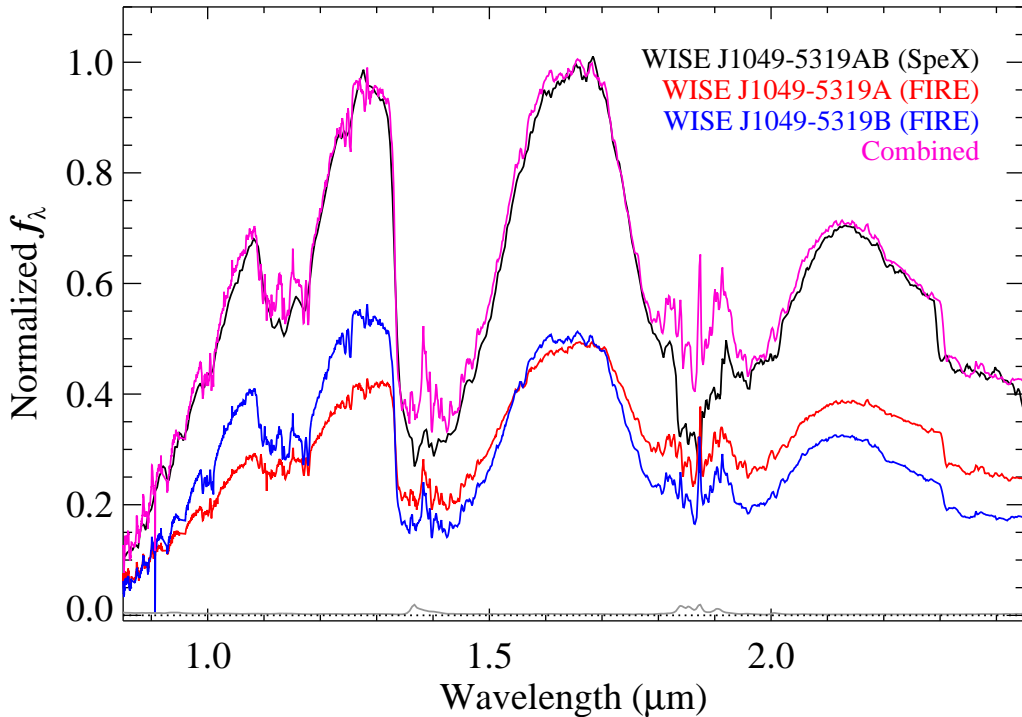
FIG. 4.— Relative flux scaling of the FIRE spectra of WISE J1049−5319A (red) and B (blue) based on the measured relative photometry (Table 2). The summed spectrum (purple) is an good match to the combined-light SpeX spectrum of the system (black; reddened by $A_V = 0.6$ to account for differential color refraction). Note that the secondary is brighter than the primary between 0.95–1.3 μm and 1.55–1.70 μm. The relative spectrophotometric magnitudes (MKO system) of the combination shown are $\Delta J = −0.25$, $\Delta H = 0.02$ and $\Delta K = 0.26$.

of WISE J1049−5319AB appear to rule out membership in any of the known local young associations with the possible exception of the 40 Myr Argus association (Mamajek 2013; Zuckerman et al. 2011). However, other than the Li I line in the optical spectrum of the primary, which sets a maximum age for the system of ∼4.5 Gyr (assuming $M_1 < 0.065$ $M_\odot$, $T_{eff} \approx 1350$ K and evolutionary models from Baraffe et al. 2003), there are no obvious indicators of low surface gravity in the low-resolution spectra of these sources. We therefore conclude that thick clouds is the more likely interpretation for the red colors.

Thick clouds may explain why WISE J1049−5319AB is a flux reversal binary. Excess cloud opacity in the primary suppresses its 1 μm flux, whereas reduced cloud opacity in the secondary allows light to emerge from deeper, hotter layers at these wavelengths, making this component relatively brighter. This argument has been made to explain the relative brightnesses of other flux-reversal binaries, but this is the first time resolved spectroscopy has been reported for such a system. Cloud-induced variations in the degree of flux reversal have also been previously suggested among candidate L/T transition spectral binaries (Burgasser et al. 2010a).

Why would there be a difference in the cloud properties of these coeval brown dwarfs? Overall color trends among L and T dwarfs suggest that this binary may simply straddle the evolutionary stage during which mineral clouds are disrupted, and the presumably lower-mass and lower-temperature secondary has begun to lose its clouds

first. Note that the mass differential between the components could potentially constrain the timescale over which this evolutionary phase occurs (Burgasser 2007). An alternate—or possibly concurrent—hypothesis is that these two brown dwarfs have different cloud properties due to other factors; e.g., differences in surface gravity, rotation rate or viewing orientation (metallicity or age differences are assumed negligible). In this case, the thermal evolution of the cloudy primary may have slowed due to its greater condensate opacity (Saumon & Marley 2008), potentially leading to a situation in which the lower-temperature secondary is the *more* massive component of the system.

These hypotheses are potentially testable for this system, as its relatively tight separation of (3.13±0.25 AU) makes it a promising (and rare) target for individual component mass measurements through astrometric and radial velocity (RV) orbital mapping. Assuming a true semi-major axis of roughly 4 AU and equal component masses of 0.04–0.065 $M_\odot$ (appropriate for $T_{eff} \approx 1300$–1350 K and ages of 1–4.5 Gyr; Stephens et al. 2009; Baraffe et al. 2003), this system has a likely orbital period estimate of 22–28 yr, implying astrometric orbital motion of up to 0.''3 per year and in-plane RV variability amplitudes of 0.7–0.8 km s^{-1} (corresponding to RV differences of up to 1.6 km s^{-1}). The RV velocity measurements are potentially feasible with current instrumentation (Bean et al. 2010; Blake et al. 2010), and the relatively dense stellar field around WISE J1049−5319AB means that astrometric motion should be easily measur-
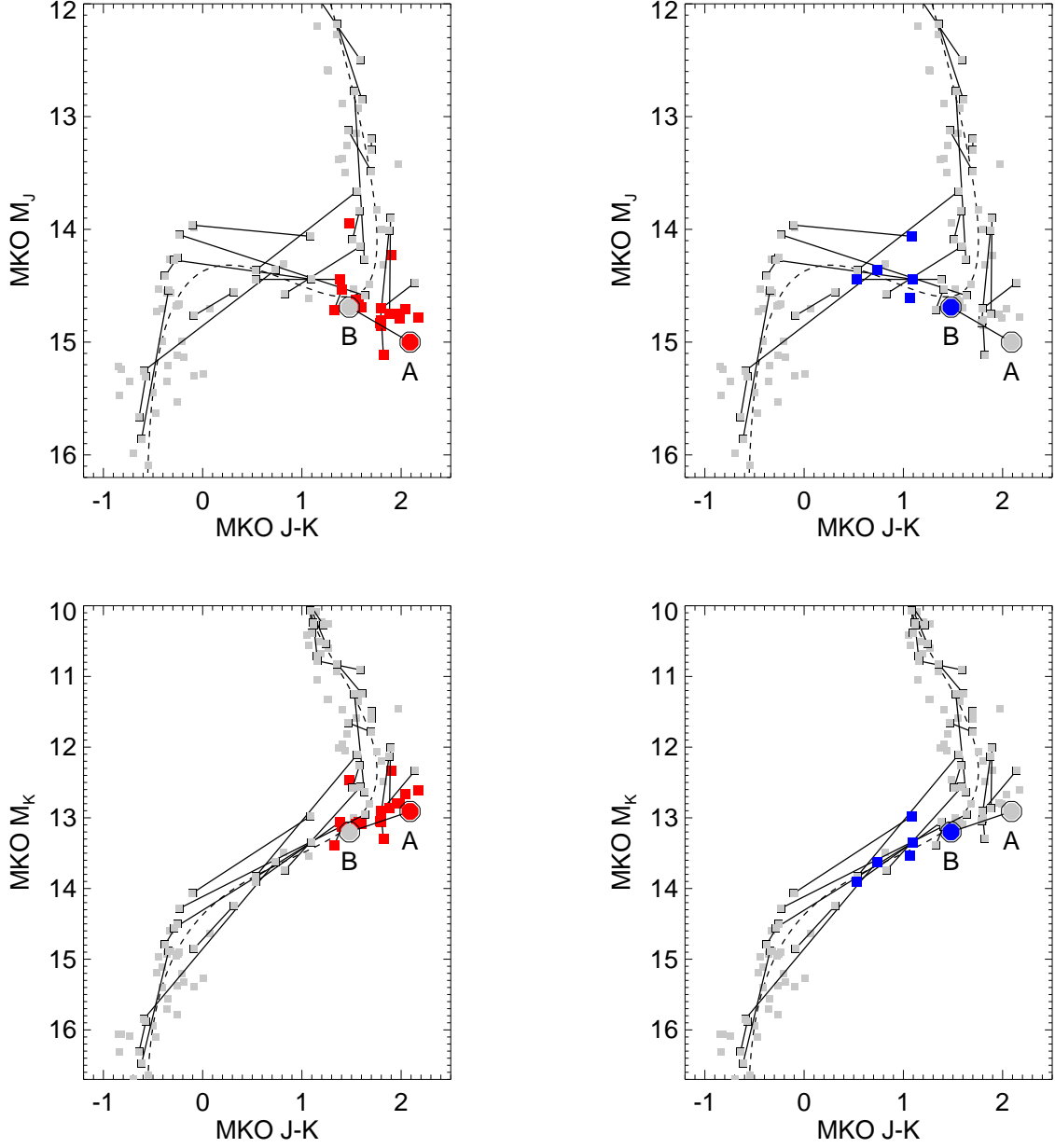
FIG. 5.— Near-infrared color-magnitude diagrams (top: M_J versus $J − K$; bottom: M_K versus $J − K$) for field L and T dwarfs with reported parallax measurements having absolute magnitude and color uncertainties ≤0.3 mag. Subdwarfs and young brown dwarfs are excluded. Components of binary systems (including WISE J1049−5319AB) are indicated by outlined symbols and connected by solid lines. L7-L8 dwarfs are highlighted in the left panels; T0-T1 dwarfs in the right panels. WISE J1049−5319A and B are somewhat redder and fainter than their equivalently classified counterparts. Mean color-magnitude trends from Dupuy & Liu (2012) are delineated by dashed lines.

able over the course of a single year.

REFERENCES

Ackerman, A. S., & Marley, M. S. 2001, ApJ, 556, 872
Allard, F., Hauschildt, P. H., Alexander, D. R., Tamanai, A., & Schweitzer, A. 2001, ApJ, 556, 357
Baraffe, I., Chabrier, G., Barman, T. S., Allard, F., & Hauschildt, P. H. 2003, A&A, 402, 701

Barman, T. S., Macintosh, B., Konopacky, Q. M., & Marois, C. 2011, ApJ, 733, 65
Bean, J. L., Seifahrt, A., Hartman, H., Nilsson, H., Wiedemann, G., Reiners, A., Dreizler, S., & Henry, T. J. 2010, ApJ, 713, 410

Blake, C. H., Charbonneau, D., & White, R. J. 2010, ApJ, 723, 684

Burgasser, A. J. 2007, ApJ, 659, 655

Burgasser, A. J., Cruz, K. L., Cushing, M., Gelino, C. R., Looper, D. L., Faherty, J. K., Kirkpatrick, J. D., & Reid, I. N. 2010a, ApJ, 710, 1142

Burgasser, A. J., Geballe, T. R., Leggett, S. K., Kirkpatrick, J. D., & Golimowski, D. A. 2006a, ApJ, 637, 1067

Burgasser, A. J., Kirkpatrick, J. D., Cruz, K. L., Reid, I. N., Leggett, S. K., Liebert, J., Burrows, A., & Brown, M. E. 2006b, ApJS, 166, 585

Burgasser, A. J., Marley, M. S., Ackerman, A. S., Saumon, D., Lodders, K., Dahn, C. C., Harris, H. C., & Kirkpatrick, J. D. 2002, ApJ, 571, L151

Burgasser, A. J., Reid, I. N., Siegler, N., Close, L., Allen, P., Lowrance, P., & Gizis, J. 2007, Protostars and Planets V, 427

Burgasser, A. J., Simcoe, R. A., Bochanski, J. J., Saumon, D., Mamajek, E. E., Cushing, M. C., Marley, M. S., McMurtry, C., Pipher, J. L., & Forrest, W. J. 2010b, ApJ, 725, 1405

Burrows, A., Marley, M. S., & Sharp, C. M. 2000, ApJ, 531, 438

Burrows, A., & Sharp, C. M. 1999, ApJ, 512, 843

Burrows, A., Sudarsky, D., & Hubeny, I. 2006, ApJ, 640, 1063

Currie, T., Burrows, A., Itoh, Y., Matsumura, S., Fukagawa, M., Apai, D., Madhusudhan, N., Hinz, P. M., Rodigas, T. J., Kasper, M., Pyo, T., & Ogino, S. 2011, ApJ, 729, 128

Cushing, M. C., Vacca, W. D., & Rayner, J. T. 2004, PASP, 116, 362

Dupuy, T. J., & Liu, M. C. 2012, ApJS, 201, 19

Dupuy, T. J., Liu, M. C., & Ireland, M. J. 2009, ApJ, 692, 729

Faherty, J. K., Rice, E. L., Cruz, K. L., Mamajek, E. E., & Núñez, A. 2013, AJ, 145, 2

Geballe, T. R., Knapp, G. R., Leggett, S. K., Fan, X., Golimowski, D. A., Anderson, S., Brinkmann, J., Csabai, I., Gunn, J. E., Hawley, S. L., Hennessy, G., Henry, T. J., Hill, G. J., Hindsley, R. B., Ivezić, Ž., Lupton, R. H., McDaniel, A., Munn, J. A., Narayanan, V. K., Peng, E., Pier, J. R., Rockosi, C. M., Schneider, D. P., Smith, J. A., Strauss, M. A., Tsvetanov, Z. I., Uomoto, A., York, D. G., & Zheng, W. 2002, ApJ, 564, 466

Hayashi, C., & Nakano, T. 1963, Progress of Theoretical Physics, 30, 460

Kelson, D. D. 2003, PASP, 115, 688

Kirkpatrick, J. D. 2005, ARA&A, 43, 195

Kirkpatrick, J. D., Barman, T. S., Burgasser, A. J., McGovern, M. R., McLean, I. S., Tinney, C. G., & Lowrance, P. J. 2006, ApJ, 639, 1120

Kirkpatrick, J. D., Looper, D. L., Burgasser, A. J., Schurr, S. D., Cutri, R. M., Cushing, M. C., Cruz, K. L., Sweet, A. C., Knapp, G. R., Barman, T. S., Bochanski, J. J., Roellig, T. L., McLean, I. S., McGovern, M. R., & Rice, E. L. 2010, ApJS, 190, 100

Kirkpatrick, J. D., Reid, I. N., Liebert, J., Cutri, R. M., Nelson, B., Beichman, C. A., Dahn, C. C., Monet, D. G., Gizis, J. E., & Skrutskie, M. F. 1999, ApJ, 519, 802

Knapp, G. R., Leggett, S. K., Fan, X., Marley, M. S., Geballe, T. R., Golimowski, D. A., Finkbeiner, D., Gunn, J. E., Hennawi, J., Ivezić, Z., Lupton, R. H., Schlegel, D. J., Strauss, M. A., Tsvetanov, Z. I., Chiu, K., Hoversten, E. A., Glazebrook, K., Zheng, W., Hendrickson, M., Williams, C. C., Uomoto, A., Vrba, F. J., Henden, A. A., Luginbuhl, C. B., Guetter, H. H., Munn, J. A., Canzian, B., Schneider, D. P., & Brinkmann, J. 2004, AJ, 127, 3553

Konopacky, Q. M., Ghez, A. M., Barman, T. S., Rice, E. L., Bailey, J. I., White, R. J., McLean, I. S., & Duchêne, G. 2010, ApJ, 711, 1087

Kumar, S. S. 1962, AJ, 67, 579

Lane, B. F., Zapatero Osorio, M. R., Britton, M. C., Martín, E. L., & Kulkarni, S. R. 2001, ApJ, 560, 390

Leggett, S. K., Geballe, T. R., Fan, X., Schneider, D. P., Gunn, J. E., Lupton, R. H., Knapp, G. R., Strauss, M. A., McDaniel, A., Golimowski, D. A., Henry, T. J., Peng, E., Tsvetanov, Z. I., Uomoto, A., Zheng, W., Hill, G. J., Ramsey, L. W., Anderson, S. F., Annis, J. A., Bahcall, N. A., Brinkmann, J., Chen, B., Csabai, I., Fukugita, M., Hennessy, G. S., Hindsley, R. B., Ivezić, Ž., Lamb, D. Q., Munn, J. A., Pier, J. R., Schlegel, D. J., Smith, J. A., Stoughton, C., Thakar, A. R., & York, D. G. 2000, ApJ, 536, L35

Liu, M. C., Leggett, S. K., Golimowski, D. A., Chiu, K., Fan, X., Geballe, T. R., Schneider, D. P., & Brinkmann, J. 2006, ApJ, 647, 1393

Looper, D. L., Gelino, C. R., Burgasser, A. J., & Kirkpatrick, J. D. 2008a, ApJ, 685, 1183

Looper, D. L., Kirkpatrick, J. D., Cutri, R. M., Barman, T., Burgasser, A. J., Cushing, M. C., Roellig, T., McGovern, M. R., McLean, I. S., Rice, E., Swift, B. J., & Schurr, S. D. 2008b, ApJ, 686, 528

Luhman, K. L. 2013, ApJ, 767, L1

Lunine, J. I., Hubbard, W. B., Burrows, A., Wang, Y.-P., & Garlow, K. 1989, ApJ, 338, 314

Magazzu, A., Martin, E. L., & Rebolo, R. 1993, ApJ, 404, L17

Mamajek, E. E. 2013, ArXiv e-prints

Marley, M. S., Saumon, D., Cushing, M., Ackerman, A. S., Fortney, J. J., & Freedman, R. 2012, ApJ, 754, 135

Morley, C. V., Fortney, J. J., Marley, M. S., Visscher, C., Saumon, D., & Leggett, S. K. 2012, ApJ, 756, 172

Radigan, J., Jayawardhana, R., Lafrenière, D., Artigau, É., Marley, M., & Saumon, D. 2012, ApJ, 750, 105

Rayner, J. T., Toomey, D. W., Onaka, P. M., Denault, A. J., Stahlberger, W. E., Vacca, W. D., Cushing, M. C., & Wang, S. 2003, PASP, 115, 362

Rebolo, R., Martin, E. L., & Magazzu, A. 1992, ApJ, 389, L83

Saumon, D., & Marley, M. S. 2008, ApJ, 689, 1327

Simcoe, R. A., Burgasser, A. J., Bernstein, R. A., Bigelow, B. C., Fishner, J., Forrest, W. J., McMurtry, C., Pipher, J. L., Schechter, P. L., & Smith, M. 2008, in Society of Photo-Optical Instrumentation Engineers (SPIE) Conference Series, Vol. 7014, Society of Photo-Optical Instrumentation Engineers (SPIE) Conference Series

Simcoe, R. A., Burgasser, A. J., Bochanski, J. J., Schechter, P. L., Bernstein, R. A., Bigelow, B. C., Pipher, J. L., Forrest, W., McMurtry, C., Smith, M. J., & Fishner, J. 2010, in Society of Photo-Optical Instrumentation Engineers (SPIE) Conference Series, Vol. 7735, Society of Photo-Optical Instrumentation Engineers (SPIE) Conference Series

Simons, D. A., & Tokunaga, A. 2002, PASP, 114, 169

Skemer, A. J., Hinz, P. M., Esposito, S., Burrows, A., Leisenring, J., Skrutskie, M., Desidera, S., Mesa, D., Arcidiacono, C., Mannucci, F., Rodigas, T. J., Close, L., McCarthy, D., Kulesa, C., Agapito, G., Apai, D., Argomedo, J., Bailey, V., Boutsia, K., Briguglio, R., Brusa, G., Busoni, L., Claudi, R., Eisner, J., Fini, L., Follette, K. B., Garnavich, P., Gratton, R., Guerra, J. C., Hill, J. M., Hoffmann, W. F., Jones, T., Krejny, M., Males, J., Masciadri, E., Meyer, M. R., Miller, D. L., Morzinski, K., Nelson, M., Pinna, E., Puglisi, A., Quanz, S. P., Quiros-Pacheco, F., Riccardi, A., Stefanini, P., Vaitheeswaran, V., Wilson, J. C., & Xompero, M. 2012, ApJ, 753, 14

Stephens, D. C., Leggett, S. K., Cushing, M. C., Marley, M. S., Saumon, D., Geballe, T. R., Golimowski, D. A., Fan, X., & Noll, K. S. 2009, ApJ, 702, 154

Tinney, C. G., Burgasser, A. J., & Kirkpatrick, J. D. 2003, AJ, 126, 975

Tokunaga, A. T., Simons, D. A., & Vacca, W. D. 2002, PASP, 114, 180

Tsuji, T., Ohnaka, K., & Aoki, W. 1996, A&A, 305, L1+

Vacca, W. D., Cushing, M. C., & Rayner, J. T. 2003, PASP, 115, 389

Zuckerman, B., Rhee, J. H., Song, I., & Bessell, M. S. 2011, ApJ, 732, 61